^{68}Ga-PSMA-HBED-CC PET for Differential Diagnosis of Suggestive Lung Lesions in Patients with Prostate Cancer

Thomas Pyka[1], Gregor Weirich[2], Ingo Einspieler[1], Tobias Maurer[3], Jörg Theisen[4], Georgios Hatzichristodoulou[3], Kristina Schwamborn[2], Markus Schwaiger[1], and Matthias Eiber[1]

[1]Department of Nuclear Medicine, Klinikum Rechts der Isar der TU München, Munich, Germany; [2]Institute of Pathology, Klinikum Rechts der Isar der TU München, Munich, Germany; [3]Department of Urology, Klinikum Rechts der Isar der TU München, Munich, Germany; and [4]Department of Surgery, Klinikum Rechts der Isar der TU München, Munich, Germany

In prostate cancer (PC) patients, the differentiation between lung metastases and lesions of different origin, for example, primary lung cancer, is a common clinical question. Herein, we investigated the use of Glu-NH-CO-NH-Lys(Ahx)-HBED-CC (^{68}Ga-PSMA-HBED-CC) for this purpose. **Methods:** PC patients (n = 1,889) undergoing ^{68}Ga-PSMA PET/CT or PET/MR scans were evaluated retrospectively for suggestive lung lesions. For up to 5 lesions per patient, location, CT diameter, CT morphology, and SUV_{max} were determined. The standard for classification was either histopathologic evaluation or, in the case of PC metastases, responsivity to antihormone therapy. A comparison of the different classes was executed by Student t test. Prostate-specific antigen and prostate-specific membrane antigen (PSMA) immunohistochemistry were performed if histologic samples were available; ^{68}Ga-PSMA autoradiography was performed on an exemplary case of PET-positive lung cancer. **Results:** Eighty-nine lesions in 45 patients were identified, of which 76 were classified as PC (39 proven, 37 highly probable), 7 as primary lung cancer, and 2 as activated tuberculosis; 4 lesions remained unclear. The mean SUV_{max} was 4.4 ± 3.9 for PC metastases and 5.6 ± 1.6 for primary lung cancer (P = 0.408). Additionally, substantial differences in SUV_{max} intraindividually were detected. The 2 tuberculous lesions showed an SUV_{max} of 7.8 and 2.5. Using immunohistochemistry, we could demonstrate PSMA expression in the neovasculature of several PSMA PET-positive lung cancers as well as in tuberculous lesions from our histologic database. **Conclusion:** Quantitative (SUV) analysis of ^{68}Ga-PSMA PET was not able to discriminate reliably between pulmonary metastases and primary lung cancer in PC patients. The reason for the unexpectedly high tracer uptake in non-PC lesions is not completely clear. PSMA expression in neovasculature provides a possible explanation for this finding; however, other contributing factors, such as tracer binding to proteins other than PSMA, cannot be excluded at present.

Key Words: ^{68}Ga-PSMA; prostate cancer; pulmonary metastasis; lung cancer

J Nucl Med 2016; 57:367–371
DOI: 10.2967/jnumed.115.164442

Radiolabeled prostate-specific membrane antigen (PSMA) ligands are increasingly used in the work-up of patients with prostate cancer (PC). PSMA, or glutamate carboxypeptidase II, is a membrane-bound protein expressed in the prostate and a variety of other tissues (*1,2*). It shows significantly elevated expression levels in PC compared with benign prostatic cells (*3*), making it a promising target for molecular imaging. Glu-NH-CO-NH-Lys(Ahx)-HBED-CC (^{68}Ga-PSMA-HBED-CC) is an extracellular PSMA inhibitor combining a urea-based binding motif with an interaction between the HBED-CC chelator and a lipophilic pocket in the extracellular PSMA domain (*4*). PET with ^{68}Ga-labeled PSMA-HBED-CC has been shown to be of high clinical value for lymph node staging and detection of local recurrence in PC patients, resulting in detection rates of up to 97% depending on prostate-specific antigen (PSA) levels (*5,6*). Although these excellent results are consistent with a high specificity based on preclinical studies (*7*), there have also been reports on tracer enhancement in benign lesions and other tumor entities (*8,9*). This phenomenon has been attributed mainly to PSMA expression in neovasculature and specialized (e.g., endocrine) cells as demonstrated by immunohistochemistry (*3*).

Visceral metastases are encountered less often than lymph node or bone metastases and occur predominantly in the later course of disease (*10*) but affect prognosis severely (*11*) and may lead to changes in the therapeutic regimen. The predominant sites of visceral metastases in a postmortem study were lung (46% of patients with distant metastases), liver (25%), pleura (21%), and adrenals (13%) (*12*). The differentiation between PC metastases and lesions of different origin using conventional imaging may be challenging and, in many cases, warrants histologic clarification. Imaging options for lung nodules are especially restricted, because only plain x-ray, CT, and ^{18}F-FDG PET are clinically established for this purpose (*13*)—the last, though, is of limited value in PC (*14*). Herein, we investigated the value of ^{68}Ga-PSMA PET for the diagnostic work-up of suggestive lung nodules in PC patients and evaluated whether the high specificity of PSMA PET can help in identifying pulmonary PC metastases.

MATERIALS AND METHODS

Patients

From a total number of 1,889 individuals who underwent ^{68}Ga-PSMA-ligand PET/CT or PET/MR for staging or restaging of PC from the institutions' database (November 2012 to March 2015), patients with suggestive pulmonary nodules in CT were extracted retrospectively. Only intrapulmonary lesions, but no thoracic lymph nodes, were analyzed. Lesions with a maximum diameter of less than 7 mm were excluded to minimize partial-volume effects in PET (*15*); in addition, lesions had to be either increasing in size compared with earlier CT scans, multiple lesions, or irregularly configured. Stable nodules compared with previous or follow-up CT without specific therapy as well as those with classic signs of benignity (fat or calcification) were excluded.

Received Jul. 24, 2015; revision accepted Oct. 28, 2015.
For correspondence or reprints contact: Thomas Pyka, Department of Nuclear Medicine, Klinikum Rechts der Isar der TU München, Ismaninger Strasse 22, 81675 Munich, Germany.
E-mail: thomas.pyka@tum.de
Published online Nov. 19, 2015.

TABLE 1
Patients (n = 45)

Characteristic	n
Age (y)	68.8 (50–83)
PSA (ng/mL)	5.67 (0.2–18,000)
Injected dose (MBq)	151 (97–236)
Classification	
PC-proven	18
By histology	7
By therapy response	11
Other entity–proven	8
Non–small cell lung cancer	7
Tuberculosis	1
PC highly probable	15
Unclear	4

Data in parentheses are ranges.

All patients gave written informed consent for the purpose of anonymized evaluation and publication of their data. The retrospective analysis was approved by the institutional review board of the Technical University of Munich (permit 5665/13).

Classification

Lesions were classified into the following groups: PC all, which was further divided into PC highly probable and PC-proven; lung cancer; other entity; and unclear (Tables 1 and 2). Diagnosis of PC metastases was proven either by histology or, if pulmonary lesions showed clear regression, by antihormone therapy. If these criteria were not fulfilled, the class PC metastases highly probable was chosen for multiple suggestive lung lesions in a patient with other distant metastases, no other known malignancy, and elevated PSA levels. Lung cancer was reserved for lesions with a conclusive histology. The class other entity was chosen for lesions with a conclusive histology or sputum analysis proving a non-PC origin. The remaining suggestive lung lesions were classified as unclear.

Synthesis and Application of ^{68}Ga-PSMA-Ligand

Images were obtained with HBED-CC (*7*) that was labeled with $^{68}Ga^{3+}$ (half-life, 67.6 min) from a ^{68}Ge/^{68}Ga radionuclide generator (iThemba Labs) by means of a fully automated module (Scintomics) and good manufacturing practice–grade disposable cassettes and reagent kit (ABX) as described previously (*16*). The final product was dissolved in isotonic phosphate-buffered saline with subsequent sterile filtration.

The ^{68}Ga-PSMA-ligand complex solution was applied to patients via an intravenous bolus (mean, 151 ± 30 MBq; range, 95–236 MBq). Variation of injected radiotracer activity was caused by the short half-life of ^{68}Ga and variable elution efficiencies obtained during the lifetime of the ^{68}Ge/^{68}Ga radionuclide generator.

Imaging Protocol

PET acquisition was started at a mean time of 54.7 ± 8.5 min after tracer injection (median, 54 min; range, 45–80 min). Forty-one patients underwent ^{68}Ga-PSMA PET/CT on a Biograph mCT scanner (Siemens Medical Solutions), and 4 patients underwent ^{68}Ga-PSMA PET/MR on a Biograph mMR scanner (Siemens Medical Solutions). PET/CT and PET/MR were performed as previously described (*5,17*). Notably, for the evaluation of lung lesions an inspiratory CT of the thorax was acquired in PET/CT and an axial contrast-enhanced T1-weighted volumetric interpolated breath-hold examination sequence in PET/MR; additional inspiratory CT acquisitions were available for all PET/MR patients. All PET images were acquired in 3-dimensional mode and reconstructed by an attenuation-weighted ordered-subsets expectation maximization algorithm (4 iterations, 8 subsets) followed by a postreconstruction smoothing gaussian filter (5 mm in full width at half maximum).

Image Analysis

For up to 5 suggestive lung lesions per patient, starting from the biggest, location, morphology, CT diameter, and SUV_{max} in PSMA PET were obtained. ^{68}Ga-PSMA-ligand PET and CT or MR images were interpreted by 1 board-certified nuclear medicine physician and 1 board-certified radiologist, followed by a final consensus interpretation.

Statistical Analysis

For the different classes of lesions as described above, SUV_{max} was analyzed, and box-and-whisker plots were created. SUV_{max} of the classes PC all and PC-proven was compared with the class lung cancer using the Student t test. Tests were performed 2-sided, and a level of

TABLE 2
Lesion Characteristics

Characteristic	All	PC all	PC-proven	Lung cancer–proven	Other/unclear
No. of lesions	89	76	39	7	6
Localization					
Right upper lobe	22	16	10	5	1
Right lower lobe	19	17	9	1	1
Middle lobe	4	4	1	0	0
Left upper lobe	25	22	14	1	2
Left lower lobe	19	17	5	0	2
Configuration					
Smooth	41	39	14	0	2
Lobulated	11	10	5	0	1
Irregular	30	26	19	1	3
Speculated	7	1	1	6	0
Mean CT diameter ± SD (mm)	12.5 ± 6.3	11.8 ± 5.6	13.2 ± 6.9	21.0 ± 9.2	11.7 ± 1.8
Mean SUV_{max} ± SD	4.3 ± 3.7	4.4 ± 3.9	5.0 ± 4.4	5.5 ± 1.9	2.7 ± 2.5

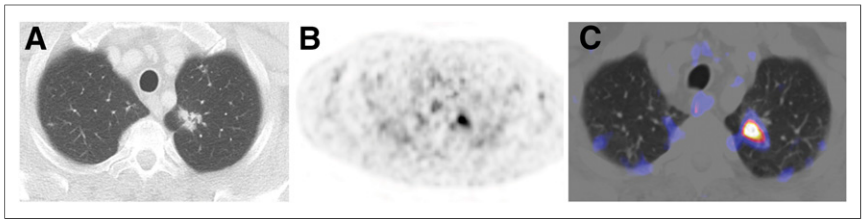

FIGURE 1. Example PSMA PET/CT scan of patient with pulmonary PC metastasis. (A) CT shows irregularly shaped lesion in left upper lobe in PC patient after radical prostatectomy, no known metastases, and PSA of 1.58 ng/mL. Lesion was subsequently biopsied and diagnosed as pulmonary PC metastasis. (B) PSMA PET is positive, with SUV_{max} of 7.1. (C) PET/CT fusion image.

FIGURE 2. Example PET/CT scans of patient with primary lung cancer (adenocarcinoma). (A) CT shows spiculated lesion in right upper lobe in PC patient after prostatectomy and suspected local recurrence; PSA was 4.09 ng/mL. (B) PSMA PET exhibits focal tracer enhancement in pulmonary lesion (SUV_{max}, 5.3) and in 2 mediastinal lymph nodes, which were histologically confirmed as primary lung cancer and associated lymph node metastases. This was the only case for which lymph node uptake was evaluated. (C) ^{18}F-FDG PET as established imaging method of choice for lung cancer shows similar enhancement in primary tumor and 2 mediastinal lymph node metastases.

significance of $\alpha = 0.05$ was used. Statistical analyses were conducted with Prism 6.1 (GraphPad Software Inc.).

Histology

For histologic evaluation, all specimens from our imaged cohort, as well as 2 exemplary cases of tuberculosis from our histologic database, were fixed in 10% buffered formalin and paraffin-embedded according to standard procedures. Tissue sections (3 μm) were subsequently stained with hematoxylin and eosin and periodic acid-Schiff stain for diagnostic purposes. Immunohistochemistry used anti-PSMA antibodies (clone 3E6 [Dako]; clone 7E11 [kindly provided by Dr. Jan Grimm, Memorial Sloan Kettering Cancer Center]) and PSA antibodies (polyclonal rabbit antihuman PSA antibody; Dako) to label PC cells. An automated immunostaining device (BenchMark XT IHC/ISH; Ventana) was used according to the manufacturer's protocol (XT ultraView DAB v3) with a citrate buffer (pH 6.0) and DAB (diaminobenzidine) as chromogen as well as hematoxylin for counterstaining.

For autoradiography, the fresh frozen tissue of 1 exemplary case of primary lung cancer, which had shown a clear signal in PSMA PET, was cryosectioned in 15-μm slices, fixed in Delauney's solution for 1 min, and air-dried. Afterward, the specimens were incubated with ^{68}Ga-PSMA-HBED-CC (30 kBq/mL) in (4-(2-hydroxyethyl)-1-piperazineethanesulfonic acid) buffer (25 mM, pH 7.4). Exposure was for 4 h on a BAS-IV TR 2025 E Tritium screen (Fujifilm).

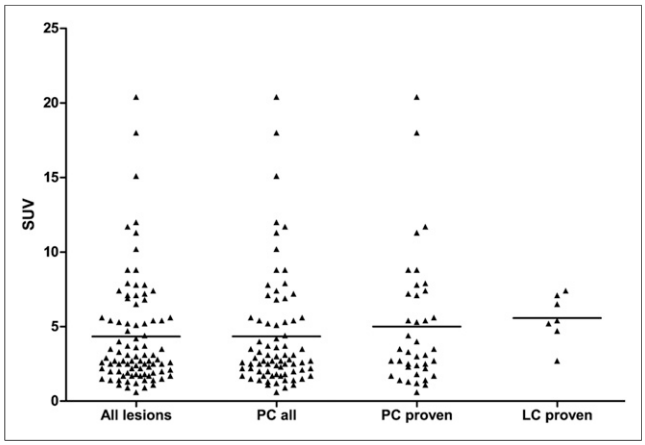

FIGURE 3. Distribution of SUV_{max} for different lesion classes. No significant difference was shown when comparing SUV_{max} distributions between groups: PC all ($n = 76$) consisting of PC-proven and PC highly probable vs. lung cancer–proven ($n = 7$) ($P = 0.408$) and PC-proven ($n = 39$) only vs. lung cancer–proven ($P = 0.780$).

RESULTS

Forty-five patients who exhibited suggestive lung lesions were identified. According to the criteria defined above, in 18 patients lesions were classified as PC-proven, in 15 as PC highly probable, and in 8 as other entity (7 cases of lung cancer and 1 case of reactivated tuberculosis). In 3 patients, the origin of the lung lesions remained unclear. There were no cases in which multiple classifications in 1 patient were present. Patient details are listed in Table 1.

The total number of suggestive pulmonary lesions was 89. Detailed lesion characteristics are given in Table 2. Thirty-nine lesions were classified as PC-proven, 37 as PC highly probable, 7 as lung cancer–proven, and 2 as other entity (both resembling activated tuberculous lesions according to sputum analysis). Four lesions remained unclear. The mean SUV_{max} was 4.3 ± 3.7 for all lesions, 4.4 ± 3.9 for all PC metastases, 5.0 ± 4.4 for histologically proven PC metastases, and 5.6 ± 1.6 for proven primary lung carcinoma. The 2 tuberculous lesions showed an SUV_{max} of 7.8 and 2.5.

Figures 1 and 2 show imaging examples of patients with pulmonary PC metastasis (PSMA PET/CT) and primary lung cancer (PSMA and ^{18}F-FDG PET/CT). Interestingly, the latter also exhibited 2 mediastinal lymph nodes, which were positive in both PSMA and ^{18}F-FDG PET scans and represented histologically proven lymph node metastases. This represents only an illustrative case for which lymph node uptake was evaluated, and it was not included into the statistical analysis.

No significant difference in SUV_{max} was observed when lung cancer was compared with all PC ($P = 0.408$; Fig. 3) or when lung cancer was compared with histologically proven PC only ($P = 0.740$), although an SUV_{max} of 8 or greater (9/89 lesions) occurred only in PC metastases. An intraindividual comparison in patients with multiple lesions showed large differences in SUV between different nodules in 1 patient (Fig. 4), which cannot be attributed solely to partial-volume effects (e.g., patient 1 exhibited an SUV_{max} from 3.1 to 20.4 while all lesions were 12–13 mm in diameter). Morphology was not distinctive either because, although all primary lung cancers had an irregular or spiculated appearance, this morphologic feature was also demonstrated in 27 (35.6%) of 76 PC metastases.

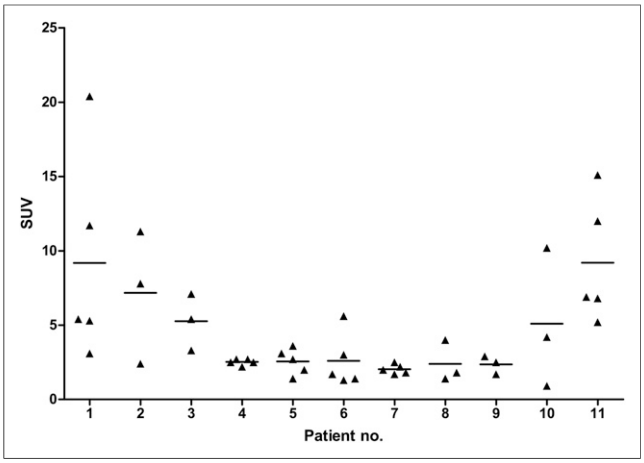

FIGURE 4. Intraindividual variability of PSMA uptake in pulmonary PC metastases. Shown is distribution of SUV_{max} for proven or probable pulmonary PC metastases in patients exhibiting 3 or more lesions.

PSMA immunohistochemistry was evaluated for the primary non–small cell lung cancers in our cohort. We could detect PSMA expression in tumor-associated neovasculature in all specimens (Fig. 5C). PSA immunohistochemistry was also performed but was negative for all samples. Furthermore, we extracted 2 cases of tuberculosis from our histologic database and could also demonstrate PSMA-positive vessels (Fig. 5D). No other cell-specific PSMA antibody binding was detected.

Postoperative PSMA autoradiography was established on frozen slices of PC tissue (Fig. 6, unpublished data). This procedure was used for an exemplary PSMA PET-positive lung tumor from the imaged cohort (SUV_{max}, 5.2) for which fresh frozen tissue was available. The PSA blood level was 0.44 ng/mL; histologic evaluation classified this tumor as a primary adenocarcinoma of the lung. Diffuse PSMA tracer binding was detected in autoradiography, which was apparently not limited to blood vessels (Figs. 6A and 6B).

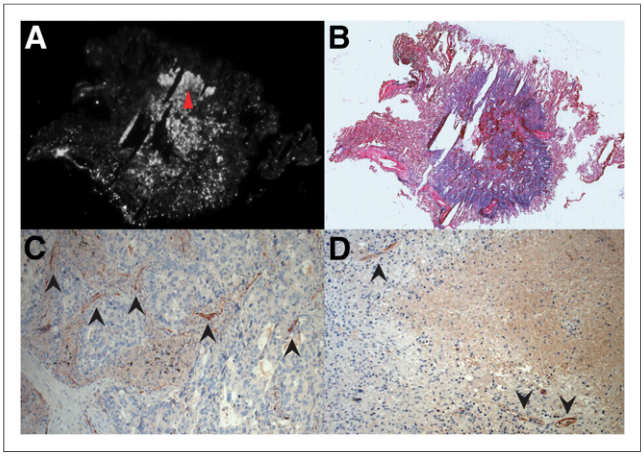

FIGURE 5. Autoradiography and PSMA immunohistochemistry of exemplary case of primary lung cancer and PSMA immunohistology of tuberculous lesion. (A) PSMA autoradiography of primary lung carcinoma from imaged cohort, which exhibited strong signal in PSMA PET (SUV_{max}, 5.2). (B) Hematoxylin and eosin stain showing tumor contours. (C) PSMA immunohistochemistry of same tumor, showing detail of tumor region with high cell density and high signal in autoradiography (red arrowhead in A), exhibiting no tumor cells with clear PSMA expression but PSMA in neovasculature (black arrowheads). (D) PSMA immunohistochemistry of case of active tuberculosis from our histologic database, showing PSMA-positive blood vessels (black arrowheads).

DISCUSSION

In this study, we retrospectively investigated the potential value of ^{68}Ga-PSMA-HBED-CC PET/CT for the differential diagnosis of suggestive lung lesions in PC patients. The differentiation of potentially malignant pulmonary lesions is of considerable clinical importance; the occurrence of distant metastases adversely affects the prognosis of PC patients and will often lead to modifications in the treatment regime, mostly systemic antihormone or chemotherapy. On the other hand, primary lung carcinoma, the second most common malignant tumor in men, is potentially curable by resection. Conventional imaging options for thoracic lesions are restricted, with only plain x-ray and CT being used in common clinical practice. The reported high specificity of PSMA PET for lymph node staging in PC patients raises expectations of a similar usefulness for the diagnosis of pulmonary metastases.

Our results do not support these expectations. Conversely, we found an unanticipated high PSMA PET uptake in primary lung tumors. Although in our cohort only PC metastases showed an SUV_{max} of greater than 8, a clear differentiation between PC metastases and primary lung cancer, for example, by an SUV_{max} cutoff, is not possible according to our data. The specificity of PSMA PET is further challenged by pronounced tracer uptake in 2 lesions resembling activated tuberculosis. Sensitivity was not as high as expected either, because several proven pulmonary PC metastases showed only faint uptake in PSMA PET, which might be explained in part by response to previous therapies. However, as a consequence, all suggestive lesions, whether exhibiting uptake in PSMA PET or not, should either be followed up by CT or PET/CT or be clarified by biopsy.

We should underline here that it was not the purpose of this study to differentiate between benign and malignant lesions by PSMA PET. Considering the inclusion criteria, it is evident that many common benign lesions, such as postinflammatory scars or granulomas, were excluded from the study. In fact, besides the 2 tuberculous lesions, there were no cases of proven benign nodules in our cohort, though some of the unclear lesions may well have been nonmalignant.

The reason for PSMA-HBED-CC tracer enhancement in non-PC lesions is not completely clear: free ^{68}Ga binding, for example, to CD71, was considered but seems rather unlikely because of the high radiochemical purity of the injected tracer. Using immunohistochemistry, we could demonstrate PSMA expression in the neovasculature of PSMA PET-positive lung carcinomas, a phenomenon that has been reported before for different tumors (*18*). Furthermore, and rather unexpectedly, we could also show PSMA immunostaining in the neovasculature of 2 exemplary cases of tuberculosis from our histologic database; reports on PSMA expression in nonneoplastic regenerative tissue can as well be found in the literature (*19*). The low density of PSMA-positive vessels, however, casts some doubt on the hypothesis that this phenomenon alone is responsible for the considerable amount of PSMA tracer uptake seen in these lesions. The doubts are substantiated by the demonstration of diffuse tracer binding in an exemplary autoradiography of a primary lung tumor from our cohort, whereas PSMA expression in lung tumor cells, though reported previously (*20*), could not be verified. This result raises the question whether binding to a substance other than PSMA might be a possible contributing factor. Natural candidate proteins would include PSMA homologs, such as glutamate carboxypeptidase III (*21,22*) or *N*-acetylated α-linked acidic dipeptidaselike protein (*23*). Further insight could be gained by performing tracer uptake

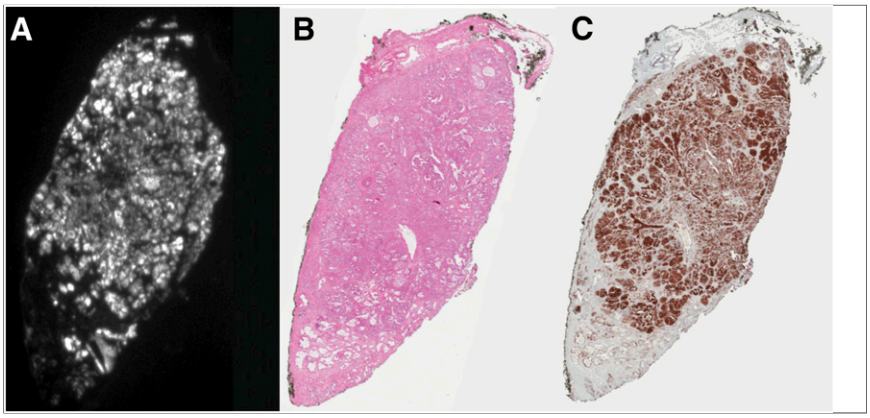

FIGURE 6. ^{68}Ga-PSMA autoradiography and PSMA immunohistochemistry of prostate carcinoma PC samples were used to establish autoradiography and immunohistology protocols. (A) PSMA autoradiography. (B) Hematoxylin and eosin stain. (C) Immunohistochemistry with anti-PSMA antibody 7E11 (aliquot kindly provided by Dr. Jan Grimm, Memorial Sloan Kettering Cancer Center).

assays on tumor cell lines, therefore excluding the effect of tracer binding to neovasculature.

Our study is limited by its retrospective nature and the relatively low number of proven non-PC lesions in the investigated cohort. In addition, we cannot exclude that, in some cases, biopsies of unclear lesions were sought because of high uptake in PET imaging, which might have induced further bias. However, we think that the most important implication—the lack of discriminative power of PSMA-HBED-CC PET imaging regarding the underlying histology of suggestive lung lesions—is not critically affected by these limitations.

CONCLUSION

Quantitative analysis of ^{68}Ga-PSMA-HBED PET was not able to discriminate reliably between pulmonary lesions of different origin in PC patients. Primary lung tumors showed unexpectedly high tracer uptake similar to PC metastases. PSMA expression in neovasculature provides a possible explanation for these findings; however, other contributing factors, such as tracer binding to proteins other than PSMA, cannot be excluded at present.

DISCLOSURE

The costs of publication of this article were defrayed in part by the payment of page charges. Therefore, and solely to indicate this fact, this article is hereby marked "advertisement" in accordance with 18 USC section 1734. This study was supported by funding from the Faculty of Medicine of the Technical University of Munich (grant KKF B11-14) and the European Union Seventh Framework Program (FP7) under grant agreement no. 294582 ERC Grant MUMI. The development of ^{68}Ga-PSMA synthesis was supported by SFB 824 (Project Z1) from the Deutsche Forschungsgemeinschaft, Bonn, Germany. The research leading to these results has received funding from the European Union Seventh Framework Program (FP7) under grant agreement no. 256984 EndoTOFPET. No other potential conflict of interest relevant to this article was reported.

REFERENCES

1. Mhawech-Fauceglia P, Zhang S, Terracciano L, et al. Prostate-specific membrane antigen (PSMA) protein expression in normal and neoplastic tissues and its sensitivity and specificity in prostate adenocarcinoma: an immunohistochemical study using multiple tumour tissue microarray technique. *Histopathology.* 2007;50:472–483.
2. Wright GL Jr, Haley C, Beckett ML, Schellhammer PF. Expression of prostate-specific membrane antigen in normal, benign, and malignant prostate tissues. *Urol Oncol.* 1995;1:18–28.
3. Silver DA, Pellicer I, Fair WR, Heston WD, Cordon-Cardo C. Prostate-specific membrane antigen expression in normal and malignant human tissues. *Clin Cancer Res.* 1997;3:81–85.
4. Kularatne SA, Zhou Z, Yang J, Post CB, Low PS. Design, synthesis, and preclinical evaluation of prostate-specific membrane antigen targeted ^{99m}Tc-radioimaging agents. *Mol Pharm.* 2009;6:790–800.
5. Eiber M, Maurer T, Souvatzoglou M, et al. Evaluation of hybrid ^{68}Ga-PSMA-ligand PET/CT in 248 patients with biochemical recurrence after radical prostatectomy. *J Nucl Med.* 2015;56:668–674.
6. Afshar-Oromieh A, Avtzi E, Giesel FL, et al. The diagnostic value of PET/CT imaging with the ^{68}Ga-labelled PSMA ligand HBED-CC in the diagnosis of recurrent prostate cancer. *Eur J Nucl Med Mol Imaging.* 2015;42:197–209.
7. Eder M, Schafer M, Bauder-Wust U, et al. ^{68}Ga-complex lipophilicity and the targeting property of a urea-based PSMA inhibitor for PET imaging. *Bioconjug Chem.* 2012;23:688–697.
8. Schwenck J, Tabatabai G, Skardelly M, et al. In vivo visualization of prostate-specific membrane antigen in glioblastoma. *Eur J Nucl Med Mol Imaging.* 2015;42:170–171.
9. Krohn T, Verburg FA, Pufe T, et al. [^{68}Ga]PSMA-HBED uptake mimicking lymph node metastasis in coeliac ganglia: an important pitfall in clinical practice. *Eur J Nucl Med Mol Imaging.* 2015;42:210–214.
10. Moschini M, Sharma V, Zattoni F, et al. Natural history of clinical recurrence patterns of lymph node-positive prostate cancer after radical prostatectomy. *Eur Urol.* 2016;69:135–142.
11. Goodman OB Jr, Flaig TW, Molina A, et al. Exploratory analysis of the visceral disease subgroup in a phase III study of abiraterone acetate in metastatic castration-resistant prostate cancer. *Prostate Cancer Prostatic Dis.* 2014;17:34–39.
12. Bubendorf L, Schopfer A, Wagner U, et al. Metastatic patterns of prostate cancer: an autopsy study of 1,589 patients. *Hum Pathol.* 2000;31:578–583.
13. Gould MK, Donington J, Lynch WR, et al. Evaluation of individuals with pulmonary nodules: when is it lung cancer? Diagnosis and management of lung cancer, 3rd ed.: American College of Chest Physicians evidence-based clinical practice guidelines. *Chest.* 2013;143:e93S-120S.
14. Jadvar H. Imaging evaluation of prostate cancer with ^{18}F-fluorodeoxyglucose PET/CT: utility and limitations. *Eur J Nucl Med Mol Imaging.* 2013;40(suppl 1):S5–S10.
15. Kessler RM, Ellis JR Jr, Eden M. Analysis of emission tomographic scan data: limitations imposed by resolution and background. *J Comput Assist Tomogr.* 1984;8:514–522.
16. Schäfer M, Bauder-Wust U, Leotta K, et al. A dimerized urea-based inhibitor of the prostate-specific membrane antigen for ^{68}Ga-PET imaging of prostate cancer. *EJNMMI Res.* 2012;2:23.
17. Souvatzoglou M, Eiber M, Martinez-Moeller A, et al. PET/MR in prostate cancer: technical aspects and potential diagnostic value. *Eur J Nucl Med Mol Imaging.* 2013;40(suppl 1):S79–S88.
18. Chang SS, Reuter VE, Heston WD, Bander NH, Grauer LS, Gaudin PB. Five different anti-prostate-specific membrane antigen (PSMA) antibodies confirm PSMA expression in tumor-associated neovasculature. *Cancer Res.* 1999;59:3192–3198.
19. Gordon IO, Tretiakova MS, Noffsinger AE, Hart J, Reuter VE, Al-Ahmadie HA. Prostate-specific membrane antigen expression in regeneration and repair. *Mod Pathol.* 2008;21:1421–1427.
20. Wang HL, Wang SS, Song WH, et al. Expression of prostate-specific membrane antigen in lung cancer cells and tumor neovasculature endothelial cells and its clinical significance. *PLoS One.* 2015;10:e0125924.
21. Hlouchová K, Barinka C, Klusak V, et al. Biochemical characterization of human glutamate carboxypeptidase III. *J Neurochem.* 2007;101:682–696.
22. Tykvart J, Schimer J, Jancarik A, et al. Design of highly potent urea-based, exosite-binding inhibitors selective for glutamate carboxypeptidase II. *J Med Chem.* 2015;58:4357–4363.
23. Tykvart J, Barinka C, Svoboda M, et al. Structural and biochemical characterization of a novel aminopeptidase from human intestine. *J Biol Chem.* 2015;290:11321–11336.